Morphological and compositional changes of chromite as it descends in the black top of a platinum group metals smelter

Oscar Rivera, Andrie Garbers-Craig [*]

Centre for Pyrometallurgy, Department of Materials Science and Metallurgical Engineering, University of Pretoria, Pretoria, South Africa

ABSTRACT

The decomposition of chromite ore in platinum group metal (PGM) concentrates and the further partitioning of chromium between PGM matte and gangue were investigated under conditions typically found in the black top of primary PGM smelters. UG–2 and Platreef PGM concentrates were fired under isothermal conditions at eight different temperatures from 800 up to 1480 °C, in sealed steel capsules. The microstructural and chemical evolution of chromite, as well as the partitioning of chromium, was studied by characterizing the PGM concentrates before and after firing, using SEM–EDS analysis. Results showed that between 800 and 1100 °C (i.e., below the solidus temperature of the silicate portion of the concentrates), the chromite particles exhibited limited reduction of Fe^{3+} to Fe^{2+} at the chromite surface, similar to the early stages of chromite reduction observed in the ferrochrome industry. After heating at 1200 °C and above, the formation of a liquid silicate was confirmed. This liquid phase acts as a solvent for the spinel components, which are subsequently transported through this liquid silicate phase to the sulfide phases and undissolved enstatite particles. At temperatures of 1300, 1400 and 1480 °C, the dissolved Al_2O_3 and FeO diffuse away from the chromite surface. This leads to the saturation of the adjacent liquid silicate in MgO and Cr_2O_3, and subsequently, $MgCr_2O_4$–rich spinel crystals precipitate. A maximum of 1.1 mass% Cr was found in the matte at 1480 °C. Chromium was transferred to the matte through reaction of the liquid matte with solid chromium-containing spinel phases and through partitioning between the liquid silicate gangue and the liquid matte.

1. Introduction

The Bushveld Igneous Complex (BIC) is the largest layered intrusion in the world. Besides hosting over half of the world reserves of platinum, 36 % of the chromium reserves and significant vanadium reserves are contained in this mineral deposit (Polyak, 2019; Schulte, 2020, 2021). Two reefs in the upper zone of the BIC are currently of importance to the platinum group metals (PGMs) industry in South Africa namely the Upper Group Chromitite No. 2 (UG–2) and Platreef reefs. The Merensky Reef was the principal source of PGMs from 1925 until the end of the twentieth century but has mostly been depleted.

The UG–2 reef is a platiniferous chromitite layer with thickness which varies from 0.4 to 1.0 m. Exploitation of this reef started in 1970 (Matthey, 2000). It consists mainly of 60–90 % (by volume) chromite [(Mg, Fe^{2+})O•(Cr, Al, Fe^{3+})$_2$ O$_3$], silicate minerals (5–30 % pyroxenes [(Fe,Mg)SiO$_3$], 1–10 % plagioclase [CaAl$_2$Si$_2$O$_8$]), as well as base metal sulfides (BMS), which are present in trace amounts (below 0.1 %). The

BMS include chalcopyrite (CuFeS$_2$), pyrrhotite (Fe$_{1-x}$S), pyrite (FeS$_2$), pentlandite [(Fe,Ni)$_9$S$_8$], and to a lesser extent millerite (NiS) (Penberthy et al., 2000). The chromium oxide (Cr$_2$O$_3$) content of the UG–2 reef varies from 30 to 35 mass%, while the average PGM content of the UG–2 reef varies between 4 and 7 g/ton.

The Platreef reef is a mineralised assemblage of pyroxenites, serpentinites and calc–silicates, with a thickness which in places reaches up to 40 m (Schouwstra et al., 2000). The Cr$_2$O$_3$ in the Platreef ore is also associated with the mineral chromite. The chromite is however present in very low concentrations, ranging between 2 and 5 vol % (Yudovskaya and Kinnaird, 2010). The base metal mineralisation and PGM concentrations are highly irregular and mainly consist of pyrrhotite, pentlandite, chalcopyrite and pyrite. PGM minerals are associated with these metal sulfides, but also with silicate minerals (pyroxenites, serpentinites, calc-silicates) and chromitite (Schouwstra et al., 2000; Klemd et al., 2016). The large-scale exploitation of the Platreef reef has been the most recent among the reefs and began only in 1993 (Schouwstra et al., 2000;

Sinisalo and Lundström, 2018).

PGMs are recovered from the ore through concentration, smelting, converting and refining processes. The concentration step involves comminution and froth flotation, after which the concentrate is dried and fed to the primary PGM smelter to form the 'black top' (BT). The BT is a bed of concentrate, ranging in height from 0.15 to 0.6 m, which floats on top of the molten slag bath (Jones, 2005; Eksteen, 2011). Its purpose is to protect the refractories in the sidewalls and roof from thermal radiation from the slag surface. A temperature gradient exists across this black top, with temperatures ranging between approximately 800 °C (at the black top – freeboard interface) to around 1500 °C (at the black top – slag interface) (Rivera Li Kao and Garbers-Craig, 2022). At the black top – slag interface, the molten silicates from the concentrate dissolve into the slag layer, while coalesced sulfides settle through the slag layer and accumulate in the matte which collects in the hearth of the smelter. As minerals in the PGM concentrate bed descend in the furnace, various phenomena occur, depending on the position and temperature of the minerals within the black top. These phenomena include dehydroxylation of hydrated phases, the decomposition, reaction and melting of silicate and sulfide phases, liquid phase sintering, as well as the coalescence of sulfides (Rivera Li Kao and Garbers-Craig, 2022).

A Fe–Ni–Cu – based matte is produced in the primary PGM smelter, which is fed to the converter. In the converter, the matte is oxidised to produce a nickel–copper – based matte, which contains the PGMs. Converter matte is either slow cooled or granulated, after which it is refined through hydrometallurgical processes to recover the base metals and PGMs (Crundwell, 2011).

Not all the chromite is removed from the ore during the flotation process, with the consequence that chromite remains in low concentrations in the UG-2 concentrate and very low concentrations in the Platreef concentrate (Rivera Li Kao and Garbers-Craig, 2022). This residual chromite has a significant impact on PGM smelting. The objective of this study was therefore to investigate the behaviour of chromite, in terms of chemical changes of the chromite and partitioning of chromium between matte and gangue, as it moves down the black top of a PGM smelter.

2. Background

In the last decades, the depletion of the Merensky Reef has led to an increased volume of UG–2 concentrate being processed. This has had far reaching implications for the smelting operation since increased concentrations of Cr_2O_3 in the slag increases its liquidus temperature to 1600 °C or even 1700 °C. Increased amounts of magnesium oxide (MgO) associated with the gangue minerals of the UG–2 reef, together with higher Cr_2O_3 concentrations, also result in the formation of [(Fe,Mg)Cr_2O_4] spinels. These spinels require higher operational temperatures in the smelter in order to decrease the viscosity of the slag. The formation of these spinels also decreases the effective volume of the smelter due to spinel build-up in the hearth (Eksteen, 2011; Eksteen et al., 2011; Nell, 2004). These negative impacts of UG–2 concentrate on PGM smelting have necessitated the blending of UG–2 concentrate with Platreef concentrate (Eksteen, 2011; Eksteen et al., 2011).

Chromite in the UG-2 ore is a complex spinel phase which can be presented by the [(Mg, Fe^{2+})O•(Cr, Al, Fe^{3+})$_2$ O$_3$] stoichiometry (Dutta and Lodhari, 2018). Chromite can form solid solutions with other oxide spinels, such as hercynite (Fe^{2+}Al$_2$O$_4$), spinel (MgAl$_2$O$_4$), magnetite (Fe^{2+}Fe$_2^{3+}$O$_4$), coulsonite (Fe^{2+}V$_2^{3+}$O$_4$), zincochromite (ZnCr$_2^{3+}$O$_4$), cochromite [(Co,Ni,Fe^{2+})(Cr,Al)$_2$O$_4$] and manganochromite [(Mn^{2+}, Fe^{2+})(Cr^{3+},V^{3+})$_2$O$_4$] (Biagioni and Pasero, 2014). All these compounds belong to the *spinel group*, which comprises a group of minerals with the general formula *AB$_2$X$_4$*, where *X* is a chalcogenide, commonly O^{2-} (oxide spinel) and more rarely S^{2-} (thiospinel) or Se^{2-} (selenospinel) (Biagioni and Pasero, 2014). In oxide spinels, *A* represents the divalent cations located in the tetrahedral sites, such as Mg, Fe^{2+}, Zn, Mn, Ni, Co, Cu and Ge; and *B* represents the trivalent cations accommodated in the

octahedral sites namely Al, Fe^{3+}, Cr^{3+}, V^{3+} and Ti^{4+} (Deer et al., 2011).

The chromium spinels commonly found in the PGM furnaces exhibit densities between 3.58 and 5.09 ton m^{-3} (Schacht, 2004). These values lie between the relative densities of the slag (2.7–3.3) and the matte (4.8–5.3). Chromium–containing spinel therefore settles through the liquid slag and accumulates at the slag/matte interface as a "mushy" layer, hindering matte settling and increasing the viscosity of the molten slag bath (Eksteen, 2011; Hundermark et al., 2011). This increase in slag viscosity is also a challenge in terms of furnace operation, as it becomes necessary to increase the furnace temperature to increase the fluidity of the slag. Higher operating temperatures imply higher energy consumption, but also compromise the integrity of the furnace due to the superheated matte, which accelerates the penetration and corrosion rates of the furnace refractories and increases the risk of damage to the copper cooling elements (Barnes and Newall, 2006; Crundwell, 2011; Nell, 2004; Schouwstra et al., 2000; Shaw et al., 2013; Sinisalo and Lundström, 2018).

Chromium–containing spinels have low solubility in the slag under prevailing conditions in the primary PGM smelters (Po$_2$ = 10^{-8}–10^{-9} bar, 1550 °C–1600 °C (Nell, 2004)), but can be partially soluble in the matte (Barnes and Newall, 2006). If the concentration of Cr_2O_3 in the concentrate exceeds its solubility limit in the slag at operating temperatures, chromium–containing spinels will accumulate in the three–phase layer suspension at the slag–matte interface, will build up in the hearth, or in front of the tap holes. This is the most likely scenario, as the PGM concentrates often contain Cr_2O_3 concentrations between 0.2 and 0.5 mass% (Platreef) and 2.3–5.0 mass% (UG–2) (Barnes and Newall, 2006; Eksteen et al., 2011; Jones and Kotzé, 2004; Rivera Li Kao and Garbers-Craig, 2022). The solubility of chromium in slags can be increased by increasing the temperature and reducing the oxygen potential whereby Cr^{3+} is reduced to Cr^{2+} (Nell, 2004). However, a simultaneous decrease in oxygen partial pressure and increase in the sulphur partial pressure increases the possibility of transferring chromium to the matte phase. Mphephu (2018) studied the interaction between synthetic PGM matte (16.10 % NiS, 23.41 % Cu$_2$S, 59.00 % FeS and 0.98 % CoS$_2$) and chromite, as well as chromia–based refractory aggregate grains at 1490 °C under argon atmosphere, using closed steel capsules. It was confirmed that the reaction between the aggregates and matte results in the transfer of chromium from the aggregate grains to the PGM matte.

Typical chromium concentrations in PGM concentrates, slags and mattes from the PGM industry are presented in Table 1. The preferential partitioning of chromium to the slag is evident, especially considering the higher volume of slag, where the matte fall (mass of matte produced relative to the mass of concentrate) lies between 9 and 25 % (Adams et al., 2011; R. Hundermark et al., 2014; Jones, 1999, 2005; Jones and Kotzé, 2004; Nolet, 2014; Zhang et al., 2009). Chromium partitions to the PGM mattes to a lesser extent, where it can exist as dissolved Cr or as precipitated FeCr$_2$O$_4$–rich crystals. Chromite particles can also get entrained in the matte (Beutner et al., 1989; Rivera Li Kao and Garbers-Craig, 2022).

3. Materials and methods

3.1. Materials

UG–2 (high Cr_2O_3 content) and Platreef (low Cr_2O_3 content) PGM concentrates were examined. These concentrates differ from each other in terms of the higher silicon and magnesium oxides content in the UG–2 concentrate (51.5 vs. 41.4 mass% SiO$_2$ and 24.7 vs. 15.8 mass% MgO),

Table 1
Typical chromium contents (mass%) in the concentrates, slags and mattes from the PGM industry.

Concentrates (mass% Cr$_2$O$_3$)	Slags (mass% Cr$_2$O$_3$)	Mattes (mass% Cr)
0.19–4.9	0.8–3.5	0.1–2.5

and the much higher concentration of nickel, copper and sulfur in the Platreef concentrate (4.09 vs. 0.90 mass% Ni, 2.12 vs. 0.20 mass% Cu, 12.80 vs. 1.82 mass% S) (Rivera Li Kao and Garbers-Craig, 2022). UG–2 concentrate has a higher chromium content than Platreef concentrate (1.56 vs. 0.18 mass% Cr_2O_3).

3.2. Experimental setup

The UG–2 concentrate was contained in MgO crucibles, and Platreef concentrate in SiO_2 crucibles. These crucibles were then placed inside sealed steel capsules, in order to avoid the escape of gaseous reaction products during firing. A Lenton muffle furnace with molybdenum disilicide ($MoSi_2$) heating elements was used in the experiments. The UG–2 and Platreef PGM concentrates were heated at eight different temperatures ranging from 800 to 1480 °C (in 100 °C steps). The samples were heated to the required temperature at a heating rate of 10 °C min^{-1}, and kept for 2 h at the selected temperature. The atmosphere inside the furnace was controlled by injecting argon (Ar) at a flow rate of 0.1 L min^{-1}, thereby protecting the steel capsules from oxidation. It is assumed that the Po_2 inside the capsules was controlled by the Fe/FeO (iron-wustite) buffer, while the sulphur partial pressure was controlled by the Fe/FeS (iron–troilite) buffer. The oxygen partial pressures therefore ranged from $10^{-17.8}$ bar (800 °C) to 10^{-9} bar (1480 °C), and the sulphur partial pressures from 10^{-9} bar (800 °C) to $10^{-3.5}$ bar (1480 °C). The calculated Po_2 of 10^{-9} bar at 1480 °C is similar to what has been reported in the literature for oxygen partial pressures in PGM smelters (Nell, 2004). The capsules were cooled down inside the furnace under an argon flow.

3.3. Analysis techniques

The microstructural analysis was performed using a Jeol JSM–IT300LV Scanning Electron Microscope (SEM), coupled with an Oxford X–Max 50 Energy–Dispersive X–ray Spectrometer (EDS). Both BE (Backscattered Electrons) and SE (Secondary Electrons) modes were used. Polished sections were prepared with AKASEL epoxy resin cured for 24 h (70 °C), after which the samples were ground (silicon carbide paper from 200# to 1200#) and polished using diamond suspensions (9.0, 6.0 and 1.0 μm).

The EMG (End Members Generator) 8.0 software (Ferracutti et al., 2015) was used to calculate the cation distribution on the basis of 4 oxygen atoms per formula unit (apfu), as well as the amounts of spinel end–members in the chromites. The chemical compositions of the spinels as determined by SEM–EDS analysis were used in these calculations.

3.4. Thermochemical predictions

Observed phase relations were compared against phase relations predicted by FactSage® 7.3 (Bale et al., 2016). The chemical stability of chromite at different temperatures was obtained from the Equilib module, using the FactPS and FToxid databases. The oxygen partial pressures used in the predictions were calculated from the iron–wüstite (Fe/FeO) oxygen buffer, as described in Section 3.2.

4. Results

4.1. Morphology, chemical composition and stoichiometry of chromite in the as-received PGM concentrates

Both concentrates consist of a mixture of silicates, chromite and sulfides. In both concentrates the chromite particles (Chr, Fig. 1 (a) and (b)) mainly occur as liberated polygonal (euhedral) crystals and to a lesser extent, irregular (subhedral) rounded–shaped crystals. Although some chromite particles exhibit cracks along their grain boundaries, no noticeable morphological alteration or compositional gradients were observed in either of the UG–2 and Platreef chromites.

The average area EDS analyses of chromite particles in the UG–2 and Platreef concentrates as well as their stoichiometries, as calculated from the average EDS analyses, are given in Table 2. The stoichiometries of the UG–2 and Platreef chromites are similar, with slightly lower Mg^{2+} and higher Fe^{2+} content in the UG–2 chromite. Chromite in both concentrates also contains low concentrations of Mn^{2+} and Ti^{4+}, while the UG-2 chromite also contains small amounts of V^{3+}. The chemical homogeneity of the chromite particles was evaluated through SEM–EDS analyses performed on the centre and rim of five chromite particles present in the UG–2 concentrate. The resulting stoichiometries of each zone are presented in Table 3. Despite the observed compositional variations from particle to particle, it is evident that the stoichiometries of the centre and rim of each particle are similar. This finding provides a clear indication of the homogeneity of the chromite in the concentrate.

4.2. Evolution of chromite in UG–2 concentrate with temperature

Due to the low chromite content of the Platreef concentrate, the study on the microstructural and chemical evolution of chromite with temperature was only performed on the UG–2 concentrate.

4.2.1. 800–1100 °C

The BEIs of the UG–2 concentrate fired at 800, 900, 1000 and 1100 °C are presented in Fig. 2. The reacted chromite particles did not exhibit morphological changes when fired in this temperature range, having the same euhedral and subhedral habits as the unreacted concentrate.

The average chemical compositions of the centres and rims of various chromite particles (analyzed by EDS), as well as the calculated stoichiometries of the analyzed areas, are presented in Table 4. The total iron
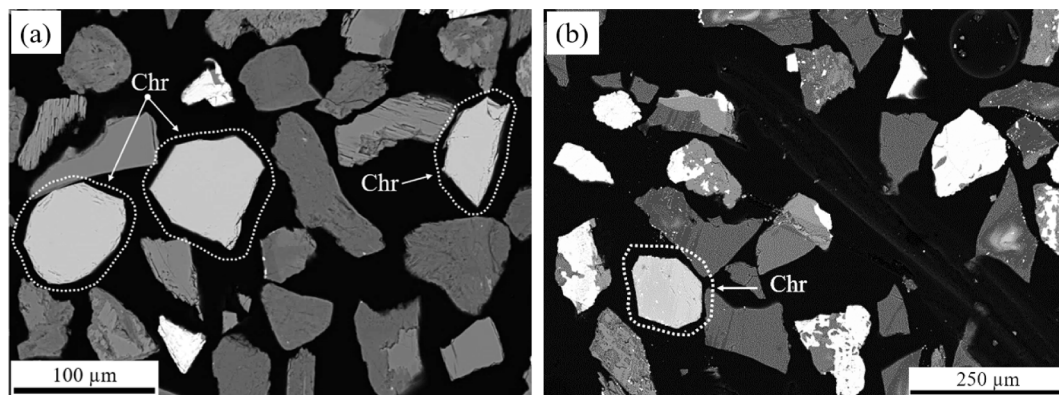

Fig. 1. BEI (backscattered electron images) of chromite in (a) UG–2 concentrate and (b) Platreef concentrate. (Dark grey: silicate minerals; Grey: chromite (Chr); Light grey / white: sulfide minerals).

Table 2

Average EDS analyses (mass%) and calculated stoichiometries of chromite in the as-received UG–2 and Platreef concentrates.

Concentrate	MgO	Iron oxide expressed as FeO	MnO	Al_2O_3	Cr_2O_3	TiO_2	V_2O_3	Total	Calculated FeO	Calculated Fe_2O_3
UG–2 *	14.86 (±2.81)	22.61 (±4.75)	0.21 (±0.10)	25.40 (±3.88)	35.79 (±2.27)	0.60 (±0.19)	0.23 (±0.07)	99.76	13.92 (±3.71)	9.66 (±2.61)
Platreef **	17.11 (±1.37)	21.09 (±1.18)	0.37 (±0.42)	30.90 (±4.24)	29.71 (±6.08)	0.71 (±0.02)	0.05 (±0.10)	99.76	11.31 (±1.91)	10.87 (±2.01)

	Stoichiometry calculated on the basis of 4 oxygen atoms
UG-2	$(Mg_{0.64}^{2+} Fe_{0.36}^{2+} Mn_{0.01}^{2+})_{\Sigma=1.01} [Al_{0.88} Cr_{0.86}^{3+} Fe_{0.23}^{3+} (Mg_{0.01}^{2+} + Ti_{0.01}^{4+})_{0.02}^{3+} V_{0.01}^{3+}]_{\Sigma=2.00} O_4$
Platreef	$(Mg_{0.71}^{2+} Fe_{0.27}^{2+} Mn_{0.01}^{2+})_{\Sigma=0.99} [Al_{1.05} Cr_{0.68}^{3+} Fe_{0.24}^{3+} (Mg_{0.02}^{2+} + Ti_{0.02}^{4+})_{0.04}^{3+}]_{\Sigma=2.01} O_4$

* Average of 51 analyses ** Average of 4 analyses.

Table 3

Calculated stoichiometries from average EDS analyses (mass%) of the centres and rims of chromite particles in the as-received UG–2 concentrate *.

	Stoichiometry calculated on the basis of 4 oxygen atoms
Centre 1	$(Mg_{0.57}^{2+} Fe_{0.42}^{2+} Mn_{0.01}^{2+})_{\Sigma=1.00} [Al_{0.84} Cr_{0.97}^{3+} Fe_{0.15}^{3+} (Mg_{0.01}^{2+} + Ti_{0.01}^{4+})_{0.01}^{3+} V_{0.01}^{3+}]_{\Sigma=1.99} O_4$
Rim 1	$(Mg_{0.58}^{2+} Fe_{0.42}^{2+})_{\Sigma=1.00} [Al_{0.82} Cr_{0.98}^{3+} Fe_{0.15}^{3+} (Mg_{0.02}^{2+} + Ti_{0.02}^{4+})_{0.04}^{3+} V_{0.01}^{3+}]_{\Sigma=2.00} O_4$
Centre 2	$(Mg_{0.37}^{2+} Fe_{0.63}^{2+})_{\Sigma=1.00} [Al_{0.71} Cr_{1.09}^{3+} Fe_{0.17}^{3+} (Mg_{0.01}^{2+} + Ti_{0.01}^{4+})_{0.02}^{3+} V_{0.01}^{3+}]_{\Sigma=2.00} O_4$
Rim 2	$(Mg_{0.38}^{2+} Fe_{0.63}^{2+})_{\Sigma=1.01} [Al_{0.71} Cr_{1.08}^{3+} Fe_{0.16}^{3+} (Mg_{0.01}^{2+} + Ti_{0.01}^{4+})_{0.02}^{3+} V_{0.01}^{3+}]_{\Sigma=1.98} O_4$
Centre 3	$(Mg_{0.57}^{2+} Fe_{0.44}^{2+})_{\Sigma=1.01} [Al_{0.87} Cr_{0.96}^{3+} Fe_{0.14}^{3+} (Mg_{0.01}^{2+} + Ti_{0.01}^{4+})_{0.02}^{3+}]_{\Sigma=1.99} O_4$
Rim 3	$(Mg_{0.55}^{2+} Fe_{0.45}^{2+})_{\Sigma=1.00} [Al_{0.87} Cr_{0.97}^{3+} Fe_{0.14}^{3+} V_{0.01}^{3+}]_{\Sigma=1.99} O_4$
Centre 4	$(Mg_{0.45}^{2+} Fe_{0.55}^{2+})_{\Sigma=1.00} [Al_{0.88} Cr_{1.04}^{3+} Fe_{0.06}^{3+} (Mg_{0.01}^{2+} + Ti_{0.01}^{4+})_{0.02}^{3+} V_{0.01}^{3+}]_{\Sigma=2.01} O_4$
Rim 4	$(Mg_{0.46}^{2+} Fe_{0.54}^{2+})_{\Sigma=1.00} [Al_{0.91} Cr_{1.01}^{3+} Fe_{0.07}^{3+} V_{0.01}^{3+}]_{\Sigma=2.00} O_4$
Centre 5	$(Mg_{0.58}^{2+} Fe_{0.42}^{2+} Mn_{0.01}^{2+})_{\Sigma=1.01} [Al_{0.90} Cr_{0.91}^{3+} Fe_{0.15}^{3+} (Mg_{0.02}^{2+} + Ti_{0.02}^{4+})_{0.04}^{3+} V_{0.01}^{3+}]_{\Sigma=2.01} O_4$
Rim 5	$(Mg_{0.59}^{2+} Fe_{0.39}^{2+})_{\Sigma=0.98} [Al_{0.92} Cr_{0.90}^{3+} Fe_{0.14}^{3+} (Mg_{0.03}^{2+} + Ti_{0.03}^{4+})_{0.06}^{3+} V_{0.01}^{3+}]_{\Sigma=2.03} O_4$

* One analysis in the centre and two analyses on the rim of each of the five analyzed chromite particles.

content, as well as Al:Cr and Mg:Fe^{2+} molar ratios in the centre of the chromite particles compared to the rims, are also shown in Table 4. It is clear that counter diffusion of Fe^{2+} and Mg^{2+} as well as Al^{3+} and Cr^{3+} took place at temperatures from 800 to 1100 °C, thereby maintaining charge neutrality in the crystal structure of the spinel. The centres of the chromite particles contained slightly higher concentrations of iron and higher concentrations of Cr^{3+} cations, while the rims contained higher concentrations of Mg^{2+} and Al^{3+}. Since the number of moles of Mg^{2+} and Fe^{2+} per four oxygen atoms in the formula unit of the spinel remained constant at 1.00, it is evident that the iron content in the centre of the chromite particle increased due to the diffusion of Fe^{2+} towards the centre of the particle. In the low-temperature zone of the black top, small amounts of Fe^{3+} was therefore reduced to Fe^{2+}, which diffused toward the centre of the chromite particles. This finding is consistent with what other authors have reported, for example, Perry et al. (1988) and Zhao et al. (2017).

4.2.2. 1200 °C

Liquid phase sintering due to the formation of a silicate liquid phase (LP) occurred at 1200 °C. The chromite particles started being surrounded by a LP and by molten matte, thereby showing a higher degree of attachment to the sintered matrix. This resulted in the bulk matte and LP picking up chromium in solution (0.37 and 0.09 mass% Cr_2O_3 in the matte and slag respectively), with some euhedral $FeCr_2O_4$ crystals precipitating on the boundaries of the matte droplets. A slight enrichment in the total iron content at the centre of the chromite particles was also verified, due to the reduction of Fe^{3+} to Fe^{2+} on the chromite surface. This reduction distorts the unit cells of the spinel structure at the surface, promoting the diffusion of Fe^{2+} cations inwards in order to maintain the charge neutrality of the spinel structure (Hazar-Yoruç, 2007; Perry et al., 1988). The diffusion of Fe^{2+} increases the iron concentration at the chromite centre, generating a coring effect, as shown in Fig. 3. The compositional differences as well as stoichiometric differences between the core and rim of this chromite particle are given in Table 5. This coring effect has been previously reported in several studies on chromite reduction (Perry et al., 1988; Weber and Eric, 1993).

The Cr_2O_3 content in the centre of the chromite increased from 36.0 mass% in the raw chromite to 40.1 mass% Cr_2O_3 at 1200 °C. This is presumably due to inward diffusion of Cr^{3+} cations, driven by the increased Fe^{2+} concentration in the centre of the particle, whereby charge neutrality is maintained. The Al_2O_3 showed no significant concentration variations between the centre and rim of the chromite particles, while the MgO content in the rim was higher than in the centre (0.75 vs 0.57 apfu).

4.2.3. 1300 °C

FactSage predicted that by increasing the heating temperature from 1200 to 1300 °C, the amount of liquid silicate that will form in the UG–2 concentrate will increase from less than 1.0 % to 26 %. The increased amount of liquid leads to a higher degree of sintering and shrinkage of the concentrate, along with the entrainment of some matte droplets within the sintered matrix. An evident softening of the chromite edges was observed at 1300 °C, especially those ones in contact with the LP, as shown in Fig. 4(a), 4(b) and 4(c). The 'softened' chromite rim contains increased amounts of Cr_2O_3 and MgO, while finely disseminated $MgCr_2O_4$–enriched spinel crystals formed around the original larger chromite particles. Several spinel fragments were also observed as smaller loose particles entrained in the gangue liquid phase (Fig. 4 (a) and (c)). The chemical compositions and stoichiometries of the different spinels are presented in Table 6.

A bright rim could be distinguished around chromite particles that were in contact with the matte phase (Fig. 5, Table 7). Chromium–enrichment of this rim was confirmed through elemental X–ray maps of this chromite particle (Fig. 6).

Sulfide phases that surround the chromite particle are enriched in chromium, with up to 1.60 mass% Cr in pentlandite and 1.1 mass% Cr in pyrrhotite, with an average of 0.11 mass% Cr in the matte. The liquid silicate phase did not contain any chromium oxide.

4.2.4. 1400 °C

After firing at 1400 °C, the chromite particles exhibit the formation of epitaxial crystals which surround the original chromite (Fig. 7). These
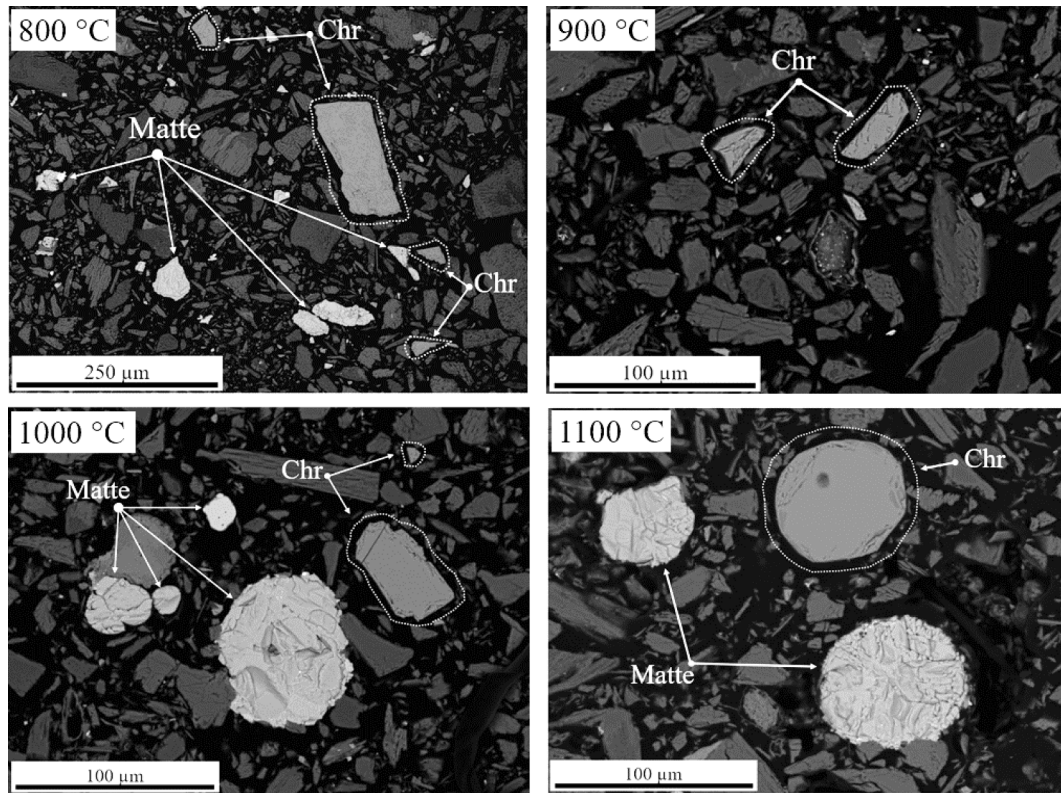
Fig. 2. BEIs of UG–2 concentrate fired at 800, 900, 1000 and 1100 °C (Chr: chromite).

Table 4
Average EDS analyses (mass%) and calculated stoichiometries of chromite particles in the UG–2 concentrate reacted at 800, 900, 1000 and 1100 °C *.

Temperature (°C)	MgO	Iron oxide expressed as FeO	MnO	Al_2O_3	Cr_2O_3	TiO_2	V_2O_3	CalculatedFeO	Calculated Fe_2O_3
800 (centre)	17.02 (±0.66)	19.69 (±0.49)	0.19 (±0.11)	28.33 (±0.56)	33.84 (±0.19)	0.60 (±0.13)	0.22 (±0.003)	10.94 (±0.90)	9.72 (±1.23)
800 (rim)	18.67 (±0.71)	16.82 (±1.61)	0.13 (±0.09)	29.47 (±1.64)	32.91 (±1.11)	0.58 (±0.09)	0.22 (±0.04)	9.82 (±0.99)	7.77 (±1.74)
900 (centre	15.61 (±1.17)	20.55 (±1.31)	0.22 (±0.08)	27.49 (±1.21)	35.26 (±1.09)	0.51 (±0.14)	0.24 (±0.12)	13.05 (±1.73)	8.33 (±0.96)
900 (rim)	15.90 (±1.37)	20.33 (±1.49)	0.20 (±0.17)	28.38 (±1.47)	34.41 (±1.35)	0.46 (±0.19)	0.20 (±0.09)	12.72 (±1.96)	8.45 (±1.18)
1000 (centre)	14.91 (±0.88)	20.63 (±0.80)	0.21 (±0.07)	28.68 (±0.58)	34.52 (±0.74)	0.71 (±0.13)	0.23 (±0.10)	14.42 (±1.56)	6.91 (±1.00)
1000 (rim)	15.50 (±0.68)	20.19 (±0.49)	0.16 (±0.08)	29.27 (±0.78)	33.60 (±0.97)	0.62 (±0.22)	0.21 (±0.01)	13.97 (±1.11)	6.92 (±1.18)
1100 (centre)	16.49 (±0.10)	19.94 (±0.15)	0.25 (±0.09)	26.82 (±0.22)	35.40 (±0.16)	0.82 (±0.002)	0.28 (±0.10)	11.71 (±0.22)	9.15 (±0.24)
1100 (rim)	16.87 (±0.37)	19.78 (±0.19)	0.21 (±0.003)	27.10 (±0.25)	34.97 (±0.45)	0.76 (±0.13)	0.31 (±0.13)	11.16 (±0.63)	9.57 (±0.51)

	Stoichiometry calculated on the basis of 4 oxygen atoms	Σn_{Fe}	n_{Al}: n_{Cr}	n_{Mg}: n_{Fe2+}
800 (centre)	$(Mg_{0.73} Fe^{2+}_{0.27} Mn^{2+}_{0.01})_{\Sigma=1.01} [Al_{0.97} Cr^{3+}_{0.78} Fe^{3+}_{0.27} (Mg^{2+}_{0.01} + Ti^{4+}_{0.01})_{0.02} V^{3+}_{0.01}]_{\Sigma=2.05} O_4$	0.54	1.24	2.70
800 (rim)	$(Mg_{0.79} Fe^{2+}_{0.25})_{\Sigma=1.04} [Al_{1.00} Cr^{3+}_{0.75} Fe^{3+}_{0.17} (Mg^{2+}_{0.01} + Ti^{4+}_{0.01})_{0.02}]_{\Sigma=1.94} O_4$	0.42	1.33	3.16
900 (centre)	$(Mg_{0.68} Fe^{2+}_{0.32})_{\Sigma=1.00} [Al_{0.96} Cr^{3+}_{0.82} Fe^{3+}_{0.19} (Mg^{2+}_{0.01} + Ti^{4+}_{0.01})_{0.02} V^{3+}_{0.01}]_{\Sigma=2.00} O_4$	0.51	1.18	2.13
900 (rim)	$(Mg_{0.69} Fe^{2+}_{0.31})_{\Sigma=1.00} [Al_{0.98} Cr^{3+}_{0.80} Fe^{3+}_{0.19} (Mg^{2+}_{0.01} + Ti^{4+}_{0.01})_{0.02}]_{\Sigma=1.99} O_4$	0.50	1.23	2.23
1000 (centre)	$(Mg_{0.64} Fe^{2+}_{0.36} Mn^{2+}_{0.01})_{\Sigma=1.01} [Al_{1.00} Cr^{3+}_{0.81} Fe^{3+}_{0.15} (Mg^{2+}_{0.02} + Ti^{4+}_{0.02})_{0.04} V^{3+}_{0.01}]_{\Sigma=2.01} O_4$	0.52	1.23	1.78
1000 (rim)	$(Mg_{0.67} Fe^{2+}_{0.34})_{\Sigma=1.01} [Al_{1.01} Cr^{3+}_{0.78} Fe^{3+}_{0.15} (Mg^{2+}_{0.01} + Ti^{4+}_{0.01})_{0.02}]_{\Sigma=1.96} O_4$	0.49	1.29	1.97
1100 (centre)	$(Mg_{0.70} Fe^{2+}_{0.29} Mn^{2+}_{0.01})_{\Sigma=1.01} [Al_{0.93} Cr^{3+}_{0.82} Fe^{3+}_{0.20} (Mg^{2+}_{0.02} + Ti^{4+}_{0.02})_{0.04} V^{3+}_{0.01}]_{\Sigma=2.00} O_4$	0.49	1.13	2.41
1100 (rim)	$(Mg_{0.72} Fe^{2+}_{0.27} Mn^{2+}_{0.01})_{\Sigma=1.00} [Al_{0.94} Cr^{3+}_{0.81} Fe^{3+}_{0.21} (Mg^{2+}_{0.02} + Ti^{4+}_{0.02})_{0.04} V^{3+}_{0.01}]_{\Sigma=2.01} O_4$	0.48	1.16	2.67

*: 800 °C sample: 7 analyses in centre, 4 rim;

900 °C sample: 10 analyses in centre, 18 on rim;

1000 °C sample: 13 analyses in centre, 24 on rim;

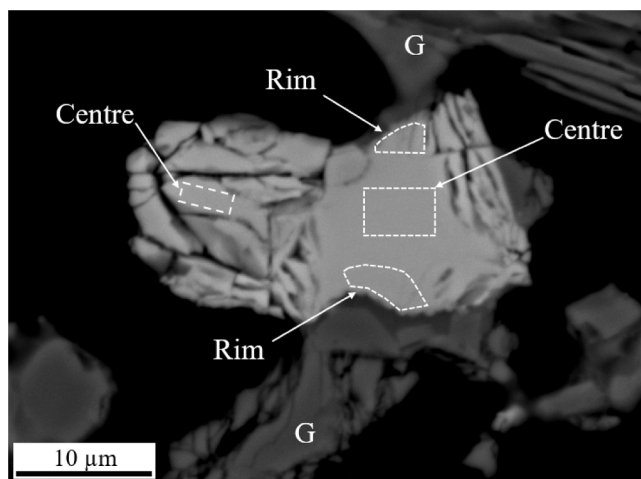1100 °C sample: 6 analyses in centre, 4 on rim.

Fig. 3. Chromite particle from UG–2 concentrate fired at 1200 °C (EDS analyses were performed on the dashed areas; G: gangue).

crystals exhibit a steep enrichment in $MgCr_2O_4$ (in some cases up to 55 %) and $FeCr_2O_4$ (up to 34 %), compared to the 28 % $MgCr_2O_4$ and 15 % $FeCr_2O_4$ found in the chromite present in the raw concentrate. The decrease in the aluminum–rich end members $MgAl_2O_4$ and $FeAl_2O_4$, from 29 % and 16 % in the concentrate to 10 % and 5 % in the epitaxial crystals is an indication of the removal of Al_2O_3 from the reacted spinel.

The centre of the chromite particles have chemical compositions

similar to the centres of the chromite particles that were reacted at 1300 °C (Figs. 5 and 6). The LP increased its chromium content from 0.0 mass% CrO at 1300 °C to 0.09 mass% CrO at 1400 °C. The chromium content in the matte increased significantly from 0.11 mass% Cr at 1300 °C to 0.28 mass% Cr at 1400 °C.

4.2.5. 1480 °C

After firing at 1480 °C, the crystals surrounding the chromite particles observed at 1400 °C have increased their epitaxy and size (Fig. 8), while the central portion of the reacted chromite started exhibiting a slightly more faceted habit compared to the chromite fired at 1400 °C. An accumulation of chromite was observed towards the bottom of the crucible (Fig. 8). This provides a clear indication that the chromite crystals did not completely dissolve, but instead settled through the liquid silicate phase. At this temperature the liquid silicate phase contained 0.20 mass% Cr_2O_3 in solution and the matte 1.10 mass% Cr.

The compositions of the centres of the chromite particles are similar to those at 1400 °C (Tables 8 and 9). The finely disseminated spinel crystals bordering the large chromite particles are MgO-Cr_2O_3 – based (Table 9) and contains $MgCr_2O_4$ (up to 73 %), with minor amounts of $FeCr_2O_4$ (12.1 %) and $MgAl_2O_4$ (8.8 %). This confirms that Al_2O_3 and FeO from the spinel dissolved into the silicate liquid phase, with the highly refractory oxides Cr_2O_3 and MgO remaining in the spinel.

4.3. Changes in cation distribution in the chromite particles with temperature

The cation distribution in the centre of the chromite particle vs. the

Table 5
Average EDS analyses (mass%) and calculated stoichiometries of chromite particle shown in Fig. 3*.

	MgO	Iron oxide expressed as FeO	MnO	Al_2O_3	Cr_2O_3	TiO_2	V_2O_3	Total	Calculated FeO	Calculated Fe2O3
Centre*	12.33 (±1.42)	25.95 (±1.13)	n.d.	20.39 (±0.23)	40.12 (±0.35)	0.65 (±0.18)	0.23 (±0.003)	99.64	17.6 (±2.28)	9.3 (±1.28)
Rim*	16.93 (±3.29)	19.67 (±2.57)	n.d.	19.87 (±0.70)	35.72 (±2.82)	0.76 (±0.004)	0.22 (±0.001)	93.14	17.3 (±0.73)	2.6 (±2.04)

Stoichiometry calculated on the basis of 4 oxygen atoms

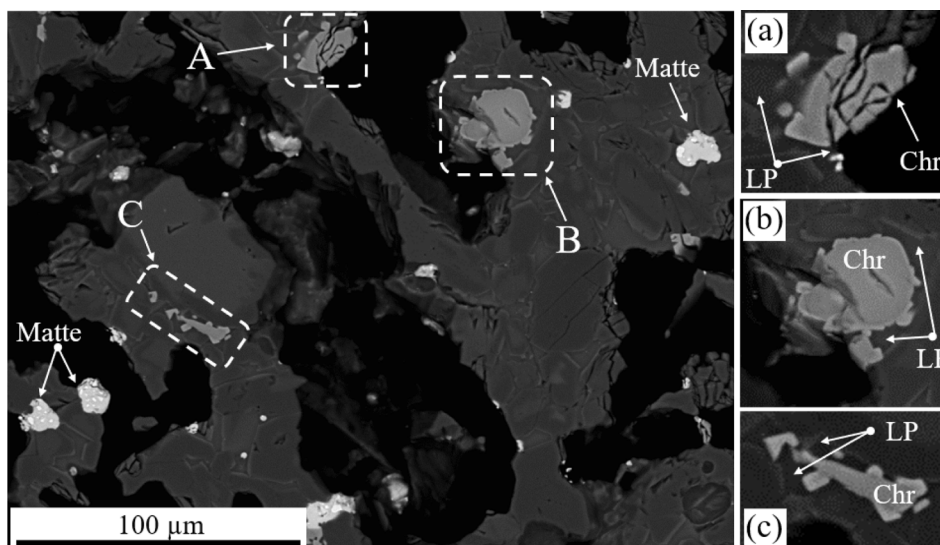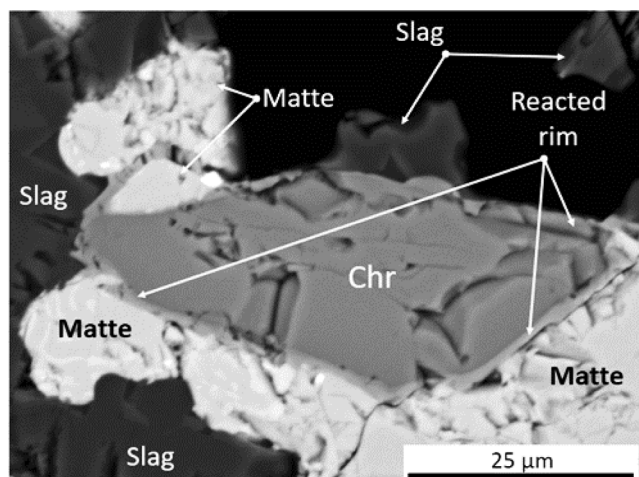| Centre	$(Mg_{0.55} Fe^{2+}_{0.46})_{\Sigma=1.01} [Al_{0.75} Cr^{3+}_{0.98} Fe^{3+}_{0.22} (Mg^{2+}_{0.02} + Ti^{4+}_{0.02})^{3+}_{0.02} V^{3+}_{0.01}]_{\Sigma=1.98} O_4$
Rim	$(Mg_{0.73} Fe^{2+}_{0.43})_{\Sigma=1.16} [Al_{0.70} Cr^{3+}_{0.84} Fe^{3+}_{0.06} (Mg^{2+}_{0.02} + Ti^{4+}_{0.02})^{3+}_{0.02} V^{3+}_{0.01}]_{\Sigma=1.63} O_4$

*: Average of 4 analyses.

Fig. 4. UG–2 concentrate fired at 1300 °C (LP: liquid phase; Chr: chromite). (a)–(c): Enlarged view of chromite particles A, B and C.

Table 6

Average EDS analyses (mass%) and calculated stoichiometries of chromite shown in Fig. 4 (1300 °C).

	MgO	Iron oxide expressed as FeO	MnO	Al_2O_3	Cr_2O_3	TiO_2	V_2O_3	Total	Calculated FeO	Calculated Fe_2O_3
Centre*	16.68	19.98	n.d.	27.27	35.16	0.49	0.21	99.79	11.84	8.93
Rim*	19.16	13.34	n.d.	17.64	47.42	0.74	0.22	98.52	7.71	6.26

Stoichiometry calculated on the basis of 4 oxygen atoms

Centre	$(Mg_{0.73} Fe^{2+}_{0.29})_{\Sigma=1.02} [Al_{0.94} Cr^{3+}_{0.82} Fe^{3+}_{0.20} (Mg^{2+}_{0.01} + Ti^{4+}_{0.01})_{0.01} V^{3+}_{0.01}]_{\Sigma=1.98} O_4$
Rim	$(Mg_{0.86} Fe^{2+}_{0.19})_{\Sigma=1.05} [Al_{0.62} Cr^{3+}_{1.12} Fe^{3+}_{0.14} (Mg^{2+}_{0.02} + Ti^{4+}_{0.02})_{0.02} V^{3+}_{0.01}]_{\Sigma=1.91} O_4$

*: Average of 2 analyses.

Fig. 5. BEI of a chromite (Chr) particle in contact with matte (1300 °C).

rim, as a function of temperature, is shown in Fig. 9(a)–9(d). The Mg content in the centre of the chromite was very variable from 800 to 1300 °C, after which a steep decrease at 1400 °C was observed up to about 0.5 atoms per formula unit (apfu) (Fig. 9(a)). The Mg and Fe^{2+} contents in the centre of the chromite particles are similar after reaction at 1400 and 1480 °C. A gradual and sustained increase in Mg occupancy and a simultaneous decrease in the Fe^{2+} content was observed in the rim of the chromite. This observation is consistent with the steep enrichment in $MgCr_2O_4$ of the spinel crystals which precipitated in the surroundings of the chromite particles at 1400 and 1480 °C.

The trivalent cation concentrations in the centre of the chromite particles remained constant at all the studied temperatures, only showing a slight increase in Cr content, with subsequent Al decrease, after firing at 1400 and 1480 °C. The rim showed a steep increase in Cr content and a simultaneous reduction in Al cations, especially after the reaction of chromite with liquid silicate, which resulted in the further formation of spinel crystals on the outer edges of the reacted chromite.

4.3.1. Chromium deportment to enstatite

Talc ($Mg_3(Si_2O_5)_2(OH)_2$) and enstatite (($Mg,Fe)_2Si_2O_6$) constitute 75.2 % of the UG–2 concentrate and 66.6 % of the Platreef concentrate.

On heating the talc starts to decompose at ~800 °C, with the formation of an additional amount of enstatite (Rivera Li Kao and Garbers-Craig, 2022). At temperatures above the solidus temperatures of the silicate portions of the concentrates (1100 and 1250 °C for Platreef and UG-2 concentrates respectively) this enstatite reacts to form part of the liquid silicate phase. Upon cooling, enstatite precipitates as primary phase from the liquid silicate phase in the Platreef concentrate and as secondary phase in the UG-2 concentrate (Rivera Li Kao and Garbers-Craig, 2022).

Enstatite present in the raw concentrate and samples that were heated from 800 to 1100 °C contained virtually no chromium (0.05–0.10 mass% CrO). However, as soon as a liquid silicate phase formed (1200 and 1300 °C), chromium was transferred through the liquid silicate phase to the enstatite, thereby increasing its chromium content to 0.18– 0.19 mass% CrO. At 1400 and 1480 °C the enstatite contained even higher concentrations of CrO (0.26 and 0.55 mass% CrO). When comparing the CrO contents of enstatites from the present study with CrO contents reported in the literature for natural and synthetic orthopyroxenes found in PGM tailings as well as in natural deposits, the observed CrO contents agrees with the reported values found in the literature for orthopyroxenes (Deer et al., 2011; Maro et al., 2016; Meyer, 2014; Riquelme Vásquez, 2016; Stalder et al., 2005).

Since the Platreef concentrate only contained 0.18 mass% Cr_2O_3, the CrO content in the enstatite was very low, remaining below 0.09 mass% CrO.

4.4. Chromium partitioning to PGM-containing matte

Chromium in the matte could either be present as dissolved chromium or in the $FeCr_2O_4$ – based spinel crystals. The concentrations of dissolved chromium in the PGM mattes as a function of temperature are shown in Fig. 10. There is a gradual increase in the chromium concentration in PGM mattes with temperature, reaching maximum values of 1.06 and 0.26 mass% Cr in UG–2 and Platreef concentrates respectively after firing at 1480 °C.

The formation of $FeCr_2O_4$ – based spinel crystals was observed in both concentrates at temperatures from 1200 °C and higher. V, Mn, Mg, Ti and Zn are also present in the spinels, but in minor amounts (Table 10). These crystals are mostly located at the perimeter of the matte droplets, are highly homogeneous and exhibit highly euhedral shapes and faceted edges. Larger and more faceted $FeCr_2O_4$ crystals could be observed as the reaction temperature increased (compare
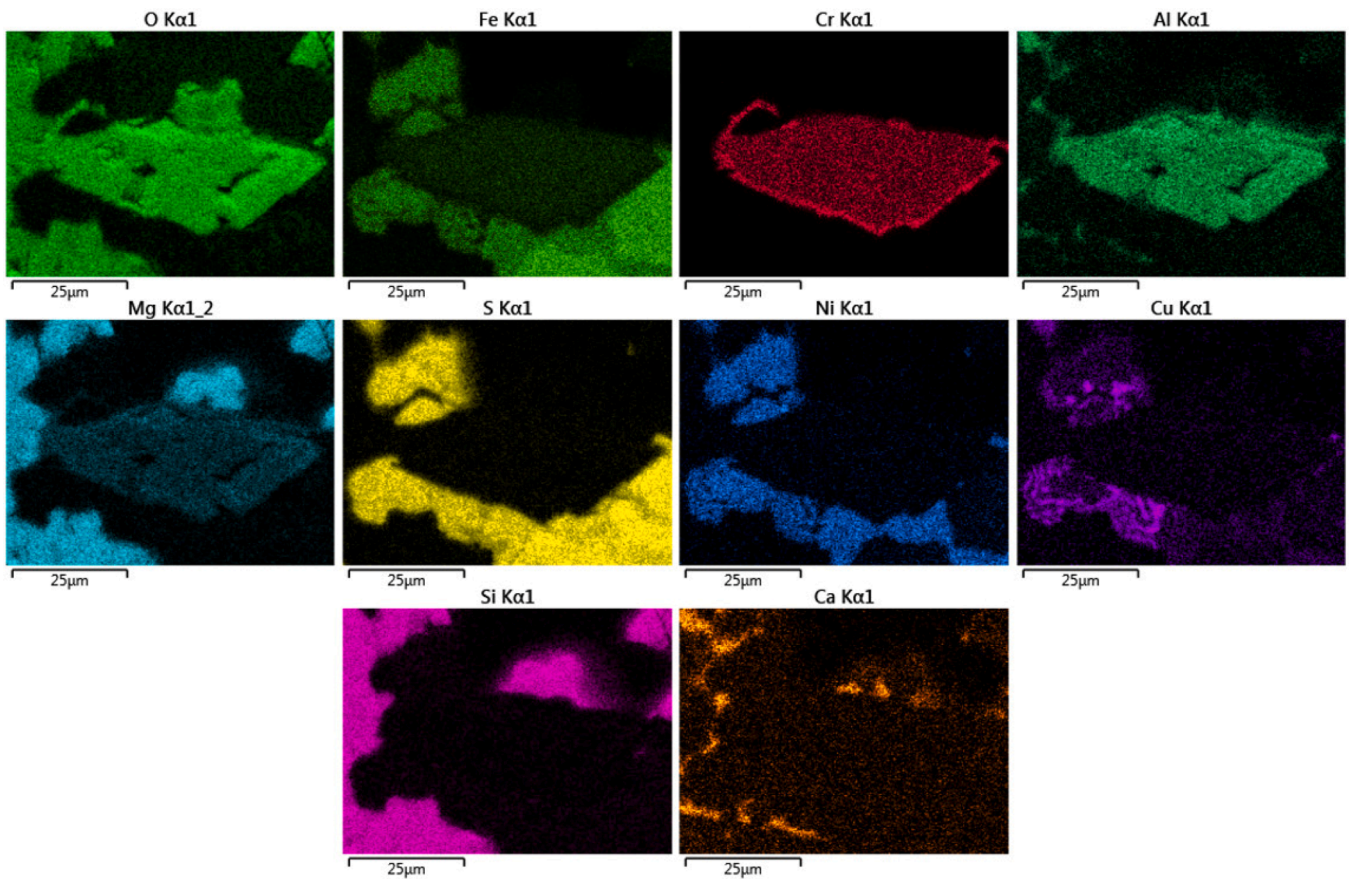
Table 7

Average EDS analyses (mass%) and calculated stoichiometries of chromite in the chromite particle in contact with matte shown in Fig. 5 (1300 °C).

	MgO	Iron oxide expressed as FeO	MnO	Al_2O_3	Cr_2O_3	TiO_2	V_2O_3	Total	Calculated FeO	Calculated Fe_2O_3
Centre*	16.60	19.70	n.d.	28.20	34.50	0.50	0.20	99.1	12.10	8.45
Rim*	16.00	19.00	0.40	4.90	57.90	1.00	0.50	99.7	9.43	10.63

Stoichiometry calculated on the basis of 4 oxygen atoms

Centre	$(Mg_{0.71} Fe^{2+}_{0.30})_{\Sigma=1.01} [Al_{0.97} Cr^{3+}_{0.80} Fe^{3+}_{0.19} (Mg^{2+}_{0.01} + Ti^{4+}_{0.01})_{0.01} V^{3+}_{0.01}]_{\Sigma=1.98} O_4$
Rim	$(Mg_{0.75} Fe^{2+}_{0.25} Mn^{2+}_{0.01})_{\Sigma=1.01} [Al_{0.19} Cr^{3+}_{1.48} Fe^{3+}_{0.26} (Mg^{2+}_{0.02} + Ti^{4+}_{0.02})_{0.02} V^{3+}_{0.01}]_{\Sigma=1.96} O_4$

*: Average of 2 analyses.

Fig. 6. Elemental X–ray maps of the chromite particle shown in Fig. 5.
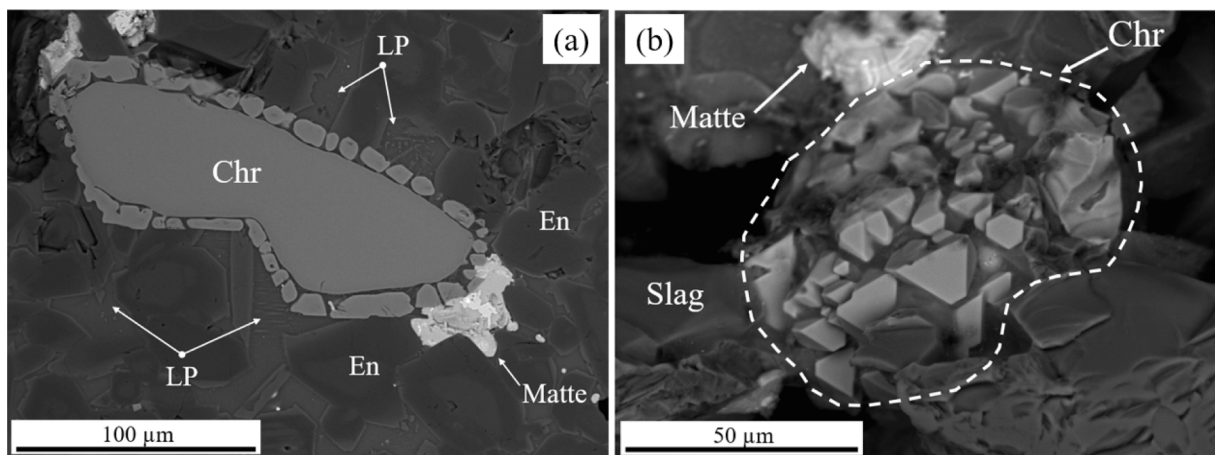

Fig. 7. UG–2 concentrate fired at 1400 °C (Chr: chromite; LP: liquid phase; En: enstatite).

Fig. 11 for UG–2 (1300 °C) with Figs. 12 and 13 for Platreef concentrate fired at 1400 and 1480 °C, respectively). The morphology of the FeCr$_2$O$_4$ – based spinel shown in Fig. 11 is similar to the spinels that precipitated from the matte. However, the high concentration of MgO suggests that it might be a partially reacted chromite particle that did not completely dissolve and was incorporated into the matte structure.

5. Discussion

5.1. Chemical and microstructural evolution of UG–2 chromite in a PGM smelter

The main transformations undergone by chromite during its evolution in the black top are schematically shown in Fig. 14(a)–(f). After firing at low temperatures (800–1100 °C), the only noticeable reaction is the limited reduction of Fe^{3+} at the surface of the chromite particles to Fe^{2+} (Fig. 14(b)). At 1200 °C the rims of the chromite particles become Fe^{2+} depleted and enriched in Mg^{2+} due to inward diffusion of Fe^{2+}
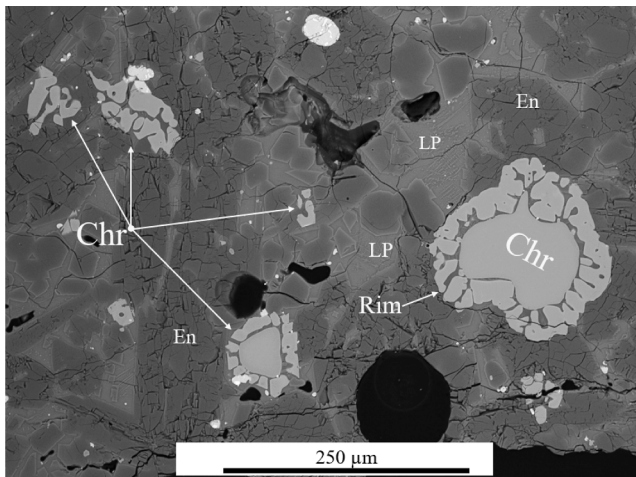
Fig. 8. UG–2 concentrate fired at 1480 °C (Chr: chromite; En: enstatite; LP: liquid silicate phase).

cations and the outward diffusion of Mg^{2+} (Fig. 14(c)). This is consistent with the initial stages of solid state reduction of chromite, as reported in the literature (Hazar-Yoruç, 2007; Lenaz et al., 2004; Weber and Eric, 2006). Two zones are therefore generated: an inner core enriched in iron, and an outer zone (rim) of lower iron contents.

Above the solidus temperature of the gangue (1200 °C) the chromite starts to react with the liquid silicate and matte phases (Fig. 14 (d)). Mainly FeO and Al_2O_3 from the rim of the chromite dissolves into the liquid silicate and diffuses away from the liquid silicate – chromite particle interface (Fig. 14 (d) and (e)). This phenomenon has been reported in several studies on chromite reduction (Dawson and Edwards, 1986; P Weber and Eric, 1992). The effective dissolution of chromite

into the surrounding liquid silicate is only achieved after a substantial amount of liquid has been formed, i.e., from 1300 °C and above. The concentration of MgO and Cr_2O_3 in the liquid silicate also increases with temperature. As the Al_2O_3 and FeO in the LP diffuse away from the chromite particle, the MgO and Cr_2O_3 contents of the liquid immediately adjacent to the chromite particle increase (Fig. 14(e)), resulting in the precipitation of $MgCr_2O_4$–enriched crystals (Fig. 14(f)). The formation of $MgCr_2O_4$–based spinels agrees with findings reported not only in the PGM industry (Bartie, 2004; Kwatara, 2006; Malan, 2015; Somerville et al., 2004), but also in ferrochrome production (Dawson and Edwards, 1986; Weber and Eric, 1993), steelmaking (Arredondo-Torres et al., 2006; Wang et al., 2013) and copper smelting (Beutner et al., 1989; Vítková et al., 2010). Magnesiochromite ($MgCr_2O_4$) is a highly stable spinel phase, with a melting point of 2400 °C (Slag Atlas Ed. 2).

5.2. Chromium partitioning

Morphological and compositional changes of chromite as it descends in the black top were investigated. Emphasis was placed on two main zones of the BT namely the low–temperature zone (800–1100 °C), where a liquid silicate phase is absent, and the high–temperature zone (1200–1480 °C), where a liquid silicate phase is present.

5.2.1. Chromium partitioning to silicate phases

Partitioning of chromium from the chromite to silicate phases (liquid silicate phase and the dominant enstatite solid solution crystals) only starts after the liquid silicate has formed. The liquid phase dissolves the spinel–forming oxides from the chromite surface, increasing and saturating the adjacent liquid in chromium oxide. Chromium dissolved in the liquid silicate phase is transferred to the enstatite solid solution phase, but on saturation also forms $MgCr_2O_4$ crystal in the vicinity of the chromite particles. Up to 0.56 mass% CrO went into solid solution with the enstatite at 1480 °C, while a maximum of 0.14 mass% CrO dissolved

Table 8
Average EDS analyses (mass%) and calculated stoichiometries of chromite in the chromite particle shown in Fig. 7.

	MgO	Iron oxide expressed as FeO	MnO	Al_2O_3	Cr_2O_3	TiO_2	V_2O_3	Total	Calculated FeO	Calculated Fe_2O_3
Fig. 7(a-1) Centre of large particle*	8.90 (±0.14)	25.60 (±0.14)	n.d.	19.40 (±0.00)	44.40 (±0.14)	1.00 (±0.00)	0.30 (±0.00)	99.60	22.61 (±0.17)	3.32 (±0.03)
Fig. 7(a-2) Crystals surrounding large particle**	12.20 (±1.83)	14.00 (±1.24)	n.d.	7.48 (±0.86)	60.13 (±3.74)	0.50 (±0.12)	0.35 (±0.10)	94.66	14.00 (±1.24)	0.00
Fig. 7(b)	9.03 (±0.15)	17.33 (±0.15)	0.33 (±0.15)	8.13 (±0.40)	62.47 (±0.91)	0.40 (±0.00)	0.43 (±0.12)	98.12	17.33 (±0.15)	0.00

Stoichiometry calculated on the basis of 4 oxygen atoms

Fig. 7(a-1)	$(Mg_{0.40} Fe^{2+}_{0.60} Mn^{2+}_{0.01})_{\Sigma=1.01} [Al_{0.73} Cr^{3+}_{1.12} Fe^{3+}_{0.08} (Mg^{2+}_{0.02} + Ti^{4+}_{0.02})^{3+}_{0.02} V^{3+}_{0.01}]_{\Sigma=1.96} O_4$
Fig. 7(a-2)	$(Mg_{0.43} Fe^{2+}_{0.48} Mn^{2+}_{0.01} Ca^{2+}_{0.01})_{\Sigma=0.93} [Al_{0.32} Cr^{3+}_{1.65} (Mg^{2+}_{0.02} + Ti^{4+}_{0.02})^{3+}_{0.02} V^{3+}_{0.01}]_{\Sigma=2.00} O_4$
Fig. 7(b)	$(Mg_{0.58} Fe^{2+}_{0.38} Ca^{2+}_{0.03})_{\Sigma=0.99} [Al_{0.29} Cr^{3+}_{1.55} (Mg^{2+}_{0.01} + Ti^{4+}_{0.01})^{3+}_{0.01} V^{3+}_{0.01}]_{\Sigma=1.86} O_4$

*: Average of 5 analyses **: 6 analyses ***: 3 analyses n.d.: Not detected.

Table 9
Average EDS analyses (mass%) and calculated stoichiometries of chromite in the chromite particles shown in Fig. 8 *.

	MgO	Iron oxide expressed as FeO	Al_2O_3	Cr_2O_3	TiO_2	V_2O_3	Total	Calculated FeO	Calculated Fe_2O_3
Fig. 8(a-1) Large chromite particle	11.20	23.40	20.20	44.10	0.80	0.30	100.00	18.93	4.97
Fig. 8(a-2) Crystals surrounding large chromite particle	18.40	8.40	5.40	67.00	0.20	0.40	99.80	5.43	3.3

Stoichiometry calculated on the basis of 4 oxygen atoms

Fig. 8(a-1)	$(Mg_{0.50} Fe^{2+}_{0.50})_{\Sigma=1.00} [Al_{0.75} Cr^{3+}_{1.09} Fe^{3+}_{0.12} (Mg^{2+}_{0.02} + Ti^{4+}_{0.02})^{3+}_{0.02} V^{3+}_{0.01}]_{\Sigma=1.99} O_4$
Fig. 8(a-2)	$(Mg_{0.86} Fe^{2+}_{0.14})_{\Sigma=1.00} [Al_{0.20} Cr^{3+}_{1.68} Fe^{3+}_{0.08} (Mg^{2+}_{0.01} + Ti^{4+}_{0.01})^{3+}_{0.01} V^{3+}_{0.01}]_{\Sigma=1.98} O_4$

*: 1 analysis in centre of large chromite particle, 1 analysis in centre of crystal surrounding large chromite particle.
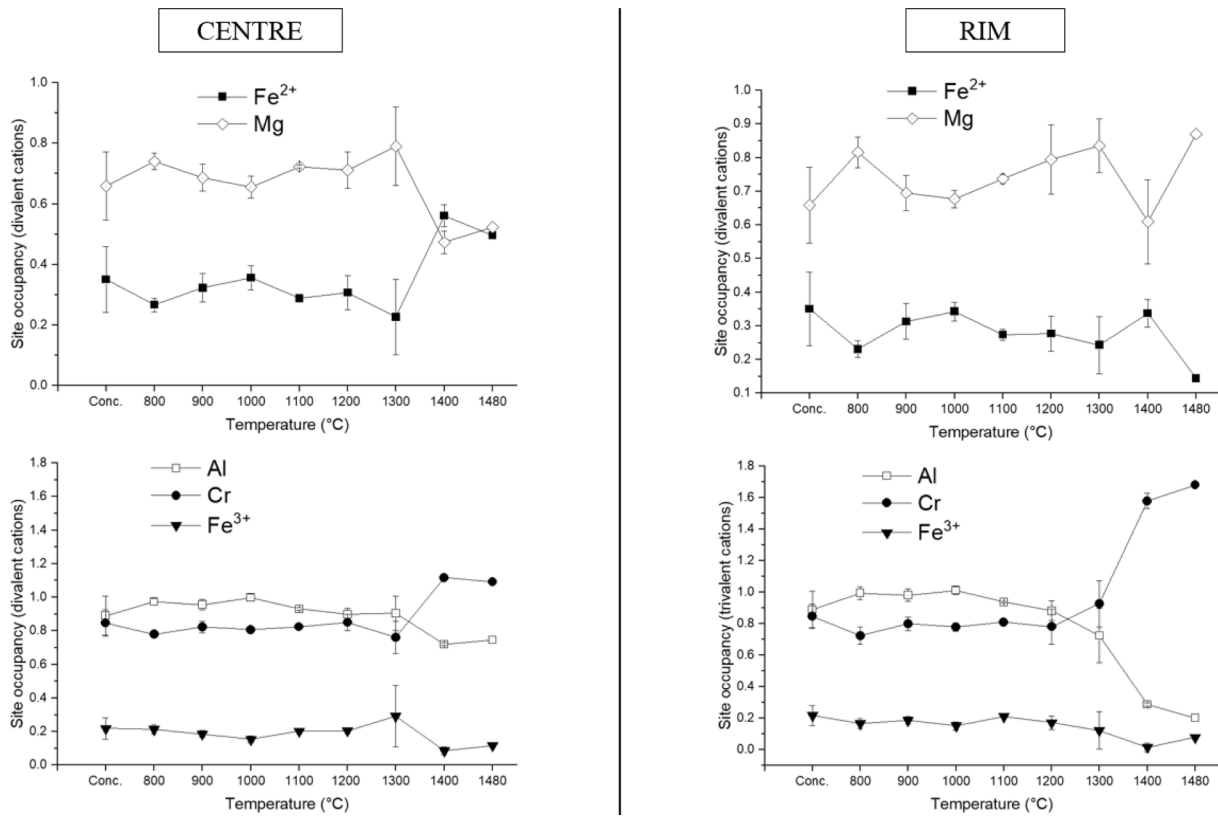
Fig. 9. Site occupancy in UG–2 chromite structure as a function of temperature ((a) divalent (centre) (b) divalent (rim) (c) trivalent (centre) and (d) trivalent (rim)).
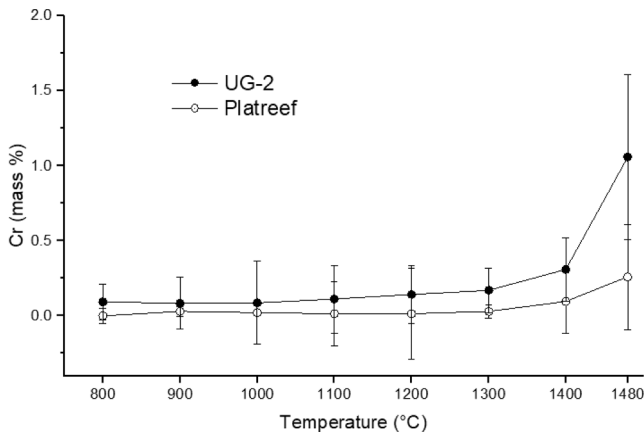

Fig. 10. Chromium concentration in the PGM mattes as a function of temperature.

in the liquid silicate at 1480 °C.

5.2.2. Chromium partitioning to matte in the black top of a PGM smelter

The higher chromite content of the UG–2 concentrate as compared to the Platreef concentrate implies that higher concentrations of chromium could partition from the chromite particles to the LP and the matte phases in the UG-2 samples (Fig. 10). Since a sustained increase in chromium concentration of the matte was observed at temperatures equal to or higher than the liquidus temperature of the matte (1000 °C), implies that partitioning of chromium to the matte starts at low temperatures via the dissolution of chromite particles into molten matte. At these temperatures a liquid silicate phase does not yet exist, as the FactSage–predicted solidus temperature of the silicate gangue of the UG–2 concentrate is 1250 °C (Rivera Li Kao and Garbers-Craig, 2022). Transfer of chromium from the chromite particles to the molten matte droplets only takes place when these two phases are coincidentally in contact with each other, as the majority of the silicate phases are still present as solid and / or altered minerals at this temperature (Fig. 15 (a)).

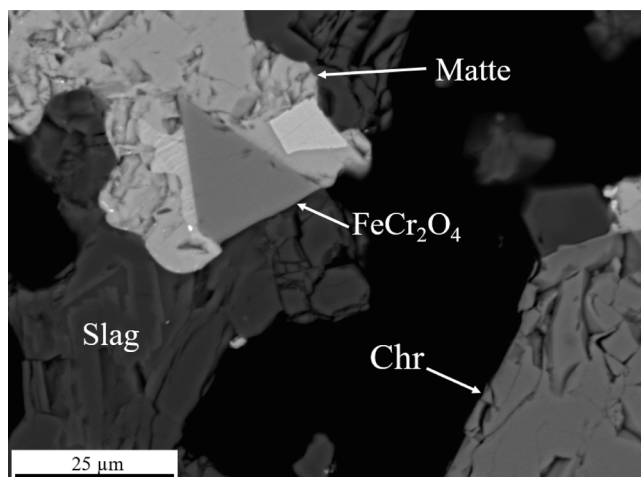Another mechanism through which chromium partitions to matte

Table 10

Average EDS analyses (mass%) and calculated stoichiometries of the spinel crystals shown in Figs. 11, 12 and 13.

	MgO	Iron oxide expressed as FeO	MnO	Al$_2$O$_3$	Cr$_2$O$_3$	TiO$_2$	V$_2$O$_3$	Total	Calculated FeO	Calculated Fe$_2$O$_3$
Fig. 11*	13.01	20.62	0.44	n.d.	61.56	2.56	0.50	98.7	12.91	8.57
Fig. 12*	1.20	29.06	1.49	0.41	64.55	n.d.	0.74	97.5	29.06	n.d.
Fig. 13*	1.01	28.68	0.64	0.40	64.12	1.42	1.98	98.3	28.68	n.d.

Stoichiometry calculated on the basis of 4 oxygen atoms

Fig. 11	$(Mg_{0.65} Fe^{2+}_{0.36} Mn^{2+}_{0.01})_{\Sigma=1.01} [Cr^{3+}_{1.64} Fe^{3+}_{0.22} Ti^{4+}_{0.07} V^{3+}_{0.01}]_{\Sigma=1.94} O_4$
Fig. 12	$(Mg_{0.07} Fe^{2+}_{0.89} Mn^{2+}_{0.05} Ni^{2+}_{0.02})_{\Sigma=1.03} [Al_{0.02} Cr^{3+}_{1.87} Fe^{3+}_{0.08} V^{3+}_{0.02}]_{\Sigma=1.99} O_4$
Fig. 13	$(Mg_{0.06} Fe^{2+}_{0.88} Mn^{2+}_{0.02} Ni^{2+}_{0.01})_{\Sigma=0.97} [Al_{0.02} Cr^{3+}_{1.87} Ti^{4+}_{0.04} V^{3+}_{0.06}]_{\Sigma=1.99} O_4$

*: Average of 3 analyses.

Fig. 11. BEI of the UG–2 concentrate fired at 1300 °C showing a FeCr$_2$O$_4$-based crystal on the boundary of a matte droplet.
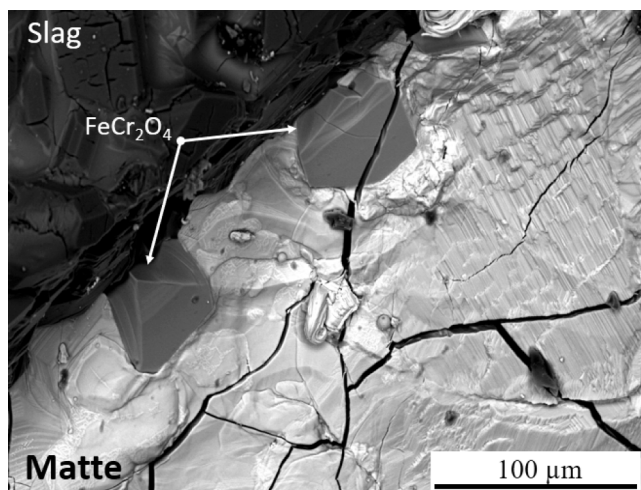

Fig. 12. BEI of the Platreef concentrate fired at 1400 °C (unpolished surface), showing FeCr$_2$O$_4$-based crystals on the edge of a matte droplet.
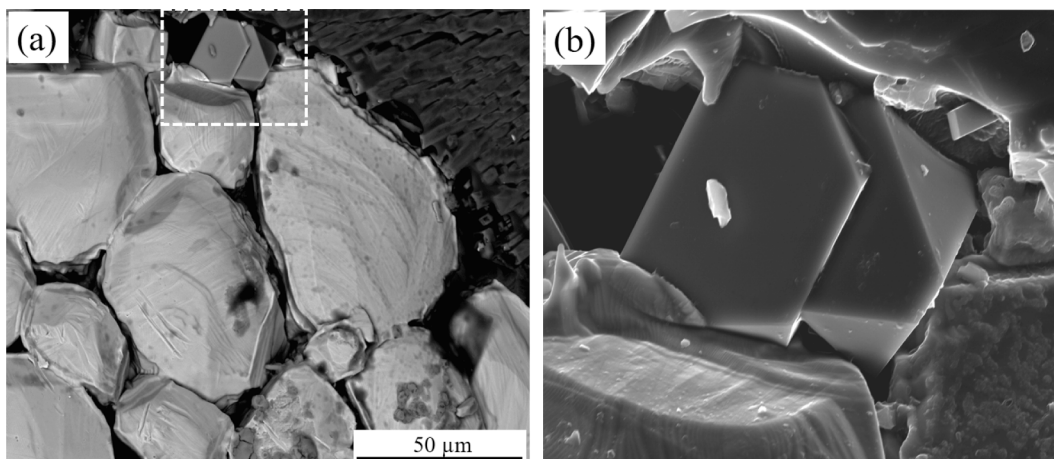
was observed at temperatures above the liquidus temperature of the liquid silicate phase (LP) (1250 °C) (Fig. 15(b) and 15(c)). This involves the dissolution of chromite into the liquid silicate phase, followed by the diffusion of the spinel–forming oxides (SFO) from the chromite particle – liquid silicate interface to the bulk of the LP (Fig. 15 (b)). Where the liquid phase is in contact with a matte droplet the chromium then partitions between the LP and matte according to thermodynamic principles (Fig. 15(c)).

The concentration of chromium in the PGM matte gradually increases with increasing temperature, but steeply increases after firing at 1400 °C (0.31 and 0.10 mass% Cr for UG–2 and Platreef, respectively) and 1480 °C (1.06 and 0.26 mass% Cr for UG–2 and Platreef, respectively). The observed chromium concentrations are consistent with reported chromium contents of between 0.1 and 2.5 mass% Cr in industrial PGM furnace mattes (Nolet, 2014).

6. Conclusions

Chromite behaviour in the black top (BT) of the PGM smelters was studied. The following conclusions could be drawn:

- When the concentrate is located in the low-temperature zone, i.e. in the upper part of the BT (800–1100 °C), the chromite particles exhibit limited reduction of Fe^{3+} to Fe^{2+} at the particle surface. This enhances the diffusion of iron towards the centre of the particle, and outward diffusion of Mg^{2+}, thereby generating a coring effect. As chromite in the concentrate descends in the BT, a silicate liquid phase starts to form at 1200 °C. This liquid silicate phase acts as a solvent which facilitates the removal of spinel–forming oxides (mainly Al$_2$O$_3$ and FeO) from the chromite surface.
- At lower positions in the BT (1300 °C and above) a MgCr$_2$O$_4$-–enriched spinel precipitates in the surroundings of the original chromite particles. This is due to (1) an increased amount of liquid silicate which enhances the dissolution of spinel–forming oxides and (2) the saturation of the adjacent liquid silicate in MgO and Cr$_2$O$_3$. Since the silicate liquid has a low solubility for Cr$_2$O$_3$, undissolved chromite particles remain in the silicate liquid phase.
- The incorporation of chromium into the liquid matte of the UG–2 concentrate becomes evident at 1100 °C due to the intimate contact between liquid matte and chromite particles provided by the liquid matte. A noticeable increase in the chromium content in the Platreef matte only occurs after a substantial amount of liquid silicate forms, which allows the transport of chromium to the liquid matte.
- In the upper BT (low-temperature zone), chromium is present in the chromite particles and, to a lesser extent, as dissolved Cr in the matte, which is in intimate contact with chromite particles. At lower
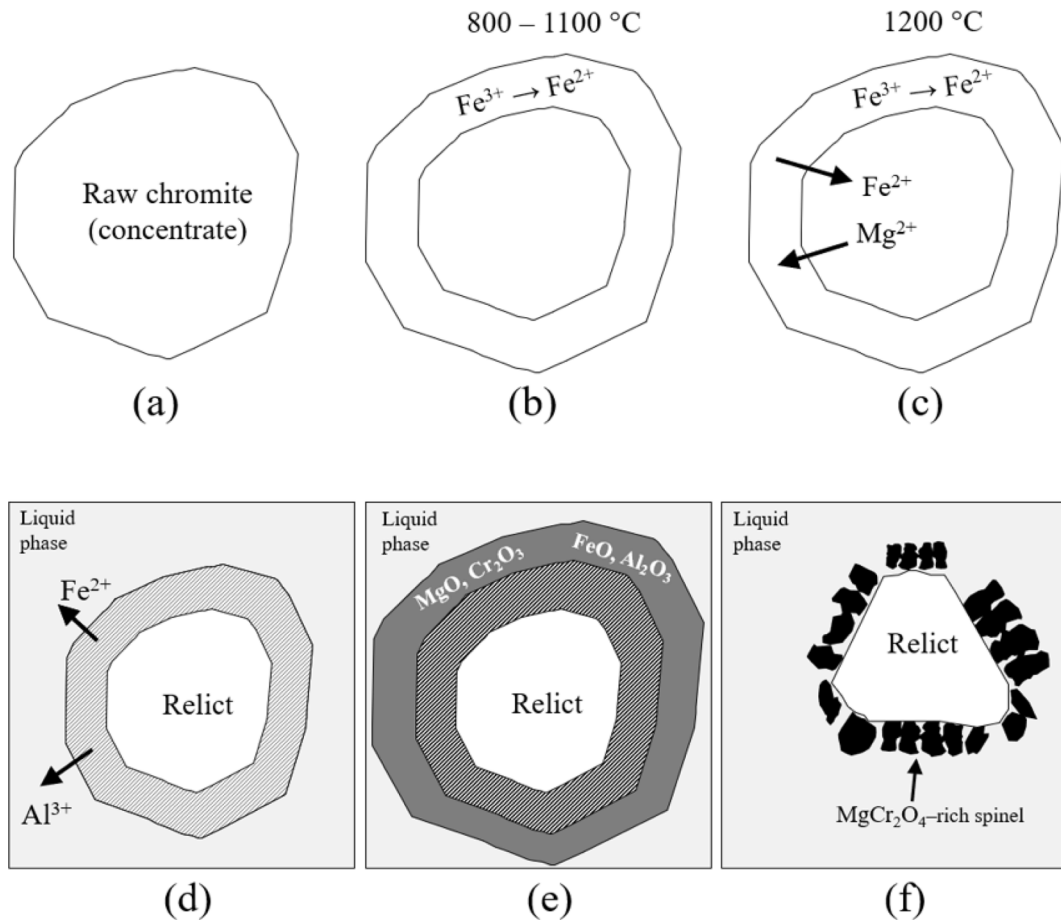

Fig. 13. Platreef concentrate fired at 1480 °C (unpolished surface) showing (a) BEI image of a FeCr$_2$O$_4$–based crystal and (b) SEI of the area marked in (a).

Fig. 14. Schematic view of the different stages of chromite evolution. (a) Raw $(Mg,Fe^{2+})[Al,Cr,Fe^{3+}]_2O_4$ chromite (b) reduction of Fe^{3+} to divalent Fe^{2+} at the chromite surface (c) counter diffusion of Fe^{2+} and Mg^{2+} (d) dissolution of spinel components in the liquid silicate and matte phases (e) saturation of the adjacent silicate liquid in MgO and Cr_2O_3 (f) precipitation and epitaxial growth of $MgCr_2O_4$–rich crystals.
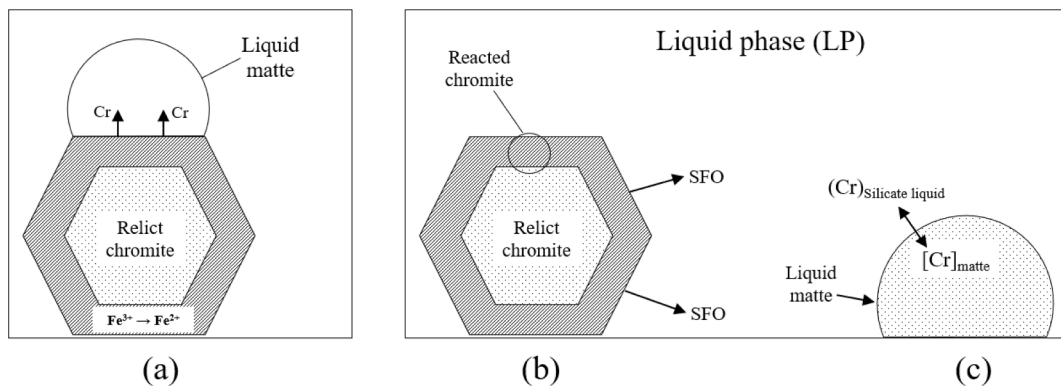

Fig. 15. Schematic presentation of the different stages through which chromium is incorporated into the matte phase: (a) Transfer of chromium into liquid matte where matte is in contact with chromite particles (b) Dissolution of chromite particles in LP and diffusion of SFO into LP; (c) Partitioning of chromium between silicate liquid and matte.

positions in the BT (high-temperature zone) chromium is (1) present as dissolved chromium in the liquid silicate phase; (2) incorporated into the matte in the form of precipitated $FeCr_2O_4$ and / or dissolved chromium (3) present as unaltered spinel with a chemical composition similar to the raw chromite and (4) in the form of a highly stable $MgCr_2O_4$–rich spinel.

- Chromium is transferred to PGM matte through interaction between chromium-containing spinels and liquid matte, as well as through partitioning between the liquid silicate gangue phase and liquid matte.

Declaration of Competing Interest

Data availability

Data are reported in the submitted paper in such a way that researchers can evaluate our findings.

Acknowledgements

References

Adams, M., Liddell, K., Holohan, T., 2011. Hydrometallurgical processing of Platreef flotation concentrate. Miner. Eng. 24 (6), 545–550. https://doi.org/10.1016/j.mineng.2010.09.009.

Arredondo-Torres, V., Romero-Serrano, A., Zeifert, B., Cruz-Rivera, J., Flores-Sánchez, P., Cruz-Ramírez, A., 2006. Stabilization of $MgCr_2O_4$ spinel in slags of the SiO_2-CaO-MgO-Cr_2O_3 system. Revista de Metalurgia (Madrid) 42 (6), 417–424. https://doi.org/10.3989/revmetalm.2006.v42.i6.40.

Bale, C.W., Bélisle, E., Chartrand, P., Decterov, S.A., Eriksson, G., Gheribi, A.E., Hack, K., Jung, I.H., Kang, Y.B., Melançon, J., Pelton, A.D., Petersen, S., Robelin, C., Sangster, J., Spencer, P., Van Ende, M.A., 2016. FactSage thermochemical software and databases, 2010–2016. CALPHAD: Comput. Coupling Phase Diagrams Thermochem. 54, 35–53. https://doi.org/10.1016/j.calphad.2016.05.002.

Barnes, A.R., Newall, A.F., 2006. Spinel removal from PGM smelting furnaces. In: Jones, R.T. (Ed.), Southern African Pyrometallurgy. South African Institute of Mining and Metallurgy, pp. 77–88.

Bartie, N.J., 2004. The Effects of Temperature, Slag Chemistry and Oxygen Partial Pressure on the Behaviour of Chromium Oxide in Melter Slags. University of Stellenbosch.

Beutner, S.P., Hagni, R.D., Robertson, D.G.C., 1989. Applied mineralogy of refinery slags. JOM 41 (4), 46–49. https://doi.org/10.1007/BF03220201.

Biagioni, C., Pasero, M., 2014. The systematics of the spinel-type minerals: An overview. Am. Mineral. 99 (7), 1254–1264. https://doi.org/10.2138/am.2014.4816.

Crundwell, F., 2011. In: Crundwell, F.K., Moats, M.S., Ramachandran, V., Robinson, T.G., Davenport, W.G. (Eds.), Extractive Metallurgy of Nickel and Cobalt. Elsevier Ltd. https://www.sciencedirect.com/book/9780080968094/extractive-metallurgy-of-nickel-cobalt-and-platinum-group-metals.

Dawson, N.F., Edwards, R.I., 1986. Factors affecting the reduction rate of chromite. In: Infacon 86 Proceedings, pp. 105–113.

Deer, W., Howie, D.J., Zussman, J., 2011. In: Bowles, J.F.W., Howie, R.A., Vaughan, D.J., Zussman, J. (Eds.) Rock-forming minerals. Volume 5A: Non-Silicates. Oxides, Hydroxides and Sulphides, second edition. The Geological Society.

Dutta, S.K., Lodhari, D.R., 2018. Extraction of Nuclear and Non-ferrous Metal. Springer Nature Singapore Pte Ltd. https://doi.org/10.1007/978-981-10-5172-2

Eksteen, J.J., 2011. A mechanistic model to predict matte temperatures during the smelting of UG2-rich blends of platinum group metal concentrates. Miner. Eng. 24 (7), 676–687. https://doi.org/10.1016/j.mineng.2010.10.017.

Eksteen, J.J., Van Beek, B., Bezuidenhout, G.A., 2011. Cracking a hard nut: an overview of Lonmin's operations directed at smelting of UG2-rich concentrate blends. J. South Afr. Inst. Min. Metall. 111 (10), 681–690.

Ferracutti, G.R., Gargiulo, M.F., Ganuza, M.L., Bjerg, E.A., Castro, S.M., 2015. Determination of the spinel group end-members based on electron microprobe analyses. Mineral. Petrol. 109 (2), 153–160. https://doi.org/10.1007/s00710-014-0363-1.

Hazar-Yoruç, A.B., 2007. Reduction mechanism of chromite spinel with carbon. Miner. Metall. Process 24 (2), 115–120. https://doi.org/10.1007/bf03403367.

Hundermark, R.J., Mncwango, S.B., Villiers, L.P., Nelson, L.R., 2011. The smelting operations of Anglo American's platinum business: an update. March, 6–9.

Hundermark, R., Nelson, L., de Villiers, B., Ndlovu, J., Mokwena, D., Mukumbe, P., Pieterse, B., Seyanund, W., van Manen, P., 2014. Redoubling Platinum Group Metal Smelting Intensity - Operational Challenges and Solutions. In: Mackey, P.J., Grimsey, E.J., Jones, R.T., Brooks, G.A. (Eds.), Celebrating the Megascale: Proceedings of the Extraction and Processing Division Symposium on Pyrometallurgy in Honor of David G.C. Robertson pp. 189–196.

Jones, R.T., 1999. Platinum smelting in South Africa. S. Afr. J. Sci. 95, 525–534.

Jones, R.T., Kotzé, I.J., 2004. DC arc smelting of difficult PGM-containing feed materials Feed materials. In: International Platinum Conference 'Platinum Adding Value,' pp. 33–36.

Jones, R.T., 2005. An overview of South African PGM smelting. In: Nickel and Cobalt 2005: Challenges in Extraction and Production, January, pp. 147–178.

Klemd, R., Herderich, T., Junge, M., Oberthür, T., Schouwstra, R., Roberts, J., 2016. Platinum-group element concentrations in base-metal sulphides from the Platreef,

Mogalakwena Platinum Mine, Bushveld Complex, South Africa. S. Afr. J. Geol. 119 (4), 623–638. https://doi.org/10.2113/gssajg.119.4.623.

Kwatara, M., 2006. Chromium Deportment in Copper Matte Equilibrated with Cr_xO-Containing Slag. University of Stellenbosch.

Malan, W.T., 2015. The recovery of platinum group metals from low-grade concentrates to an iron alloy using silicon carbide as reductant, Vol. 115, Issue 5. Stellenbosch University. doi: 10.17159/2411-9717/2015/v115n5a5.

Lenaz, D., Skogby, H., Princivalle, F., Hålenius, U., 2004. Structural changes and valence states in the $MgCr_2O_4$–$FeCr_2O_4$ solid solution series. Phys. Chem. Minerals 31, 633–642. https://doi.org/10.1007/s00269-004-0420-0.

Maro, G., Caffe, P.J., Jofré, C.B., 2016. Xenolitos Ultramáficos en Lavas Máficas Neógenas de la Puna Norte. Rev. Asoc. Geol. Argent. 73 (2), 280–291.

Matthey, J., 2000. Platinum Excavation on the UG-2 Reef in South Africa. Platinum Metals Rev. 44 (3), 105. https://www.technology.matthey.com/pdf/pmr-v44-i3-105-105.pdf.

Meyer, N.A., 2014. An Investigation into the Dissolution of Pyroxene: A Precursor to Mineral Carbonation of PGM Tailings in South Africa. University of Cape Town.

Mphephu, K., 2018. Interaction between Synthetic Platinum Furnace Matte and Different Types of Aggregate Grains. University of Pretoria.

Nell, J., 2004. Melting of platinum group metal concentrates in South Africa. J. S. Afr. Inst. Min. Metall. 104 (7), 423–428. https://www.saimm.co.za/Journal/v104n07p423.pdf.

Nolet, I., 2014. Tapping of PGM-Ni mattes: an industry survey. Furnace Tapping Conference 2014, 223–232.

Penberthy, C.J., Oosthuyzen, E.J., Merkle, R.K.W., 2000. The recovery of platinum-group elements from the UG-2 chromitite, Bushveld Complex - a mineralogical perspective. Mineral. Petrol. 68 (1–3), 213–222. https://doi.org/10.1007/s007100050010.

Perry, K.P.D., Finn, C.W.P., King, R.P., 1988. An ionic diffusion mechanism of chromite reduction. Metall. Trans. B 19 (4), 677–684. https://doi.org/10.1007/BF02659161.

Polyak, D.E., 2019. Vanadium. U.S. Geological Survey, Mineral Commodities Summaries, pp. 180–181. https://d9-wret.s3.us-west-2.amazonaws.com/assets/palladium/production/atoms/files/mcs-2019-vanad.pdf.

Riquelme Vásquez, B.A., 2016. La transición espinela-granate bajo la Región de Pali Aike, Provincia de Santa Cruz, Argentina: Un estudio a partir de xenolitos ultramáficos. Universidad de Chile.

Rivera Li Kao, O., Garbers-Craig, A., 2022. Impact of phase evolution in Platreef and UG-2 concentrates on matte drainage in the black top of a platinum group metal smelter. Mineral Process. Extract. Metall. Rev. 43(3), 326–338. doi: 10.1080/08827508.2020.1861613.

Schacht, C., 2004. In: Schacht, C. (Ed.), Refractories Handbook, first edition. Marcel Dekker, Inc. http://www.dekker.com.

Schouwstra, R.P., Kinloch, E.D., Lee, C.A., 2000. A short geological review of the Bushveld complex | Johnson Matthey Technology Review. Platin. Met. Rev. 2, 1–5. http://www.technology.matthey.com/article/44/1/33-39/.

Schulte, R., 2020. Platinum-Group Metals Statistics and Information.

Schulte, R., 2021. Chromium Statistics and Information.

Shaw, A., De Villiers, L.P.V.S., Hundermark, R.J., Ndlovu, J., Nelson, L.R., Pieterse, B., Sullivan, R., Voermann, N., Walker, C., Stober, F., McKenzie, A.D., 2013. Challenges and solutions in PGM furnace operation: High matte temperature and copper cooler corrosion. J. South Afr. Inst. Min. Metall. 113 (3), 251–261.

Sinisalo, P., Lundström, M., 2018. Refining approaches in the platinum group metal processing value chain—a review. Metals 8 (4), 203. https://doi.org/10.3390/met8040203.

Somerville, M., Wright, S., Sun, S., Jahanshahi, S., 2004. Liquidus temperature and viscosity of Melter slags. In: VII International Conference on Molten Slags Fluxes and Salts, pp. 219–224.

Stalder, R., Klemme, S., Ludwig, T., Skogby, H., 2005. Hydrogen incorporation in orthopyroxene: interaction of different trivalent cations. Contrib. Miner. Petrol. 150 (5), 473–485. https://doi.org/10.1007/s00410-005-0037-4.

Vítková, M., Ettler, V., Johan, Z., Kříbek, B., Šebek, O., Mihaljevič, M., 2010. Primary and secondary phases in copper-cobalt smelting slags from the Copperbelt Province, Zambia. Mineral. Mag. 74 (4), 581–600. https://doi.org/10.1180/minmag.2010.074.4.581.

Wang, F., Yang, Q., Xu, A., Björkman, B., 2013. Influence of Mn oxides on chemical state and leaching of chromium in EAF slag. Metall. Int. 18 (8), 88–92.

Weber, P., Eric, R., 1992. Solid-state Fluxed Reduction of LG-6 Chromite from the Bushveld Complex. Infacon 6 (1), 71–77.

Weber, P., Eric, R.H., 1993. The reduction mechanism of chromite in the presence of a silica flux. Metall. Trans. B 24 (6), 987–995. https://doi.org/10.1007/BF02660990.

Weber, P., Eric, R.H., 2006. The reduction of chromite in the presence of silica flux. Miner. Eng. 19 (3 SPEC. ISS.), 318–324. https://doi.org/10.1016/j.mineng.2005.07.010.

Yudovskaya, M.A., Kinnaird, J.A., 2010. Chromite in the Platreef (Bushveld Complex, South Africa): occurrence and evolution of its chemical composition. Miner. Deposita 45 (4), 369–391. https://doi.org/10.1007/s00126-010-0276-9.

Zhang, L., Sun, S., Jahanshahi, S., 2009. Modelling Cr containing slags for PGM smelting. In: MOLTEN 2009. Santiago, Chile.

Zhao, Q., Yan, Z., Chen, C., Chen, J., 2017. Spinels: controlled preparation, oxygen reduction/evolution reaction application, and beyond. Chem. Rev. 117 (15), 10121–10211. https://doi.org/10.1021/acs.chemrev.7b00051.